HiSST: International Conference on
High-Speed Vehicle Science Technology
26–29 November 2018, Moscow, Russia

Numerical investigation of total pressure pulsations in supersonic trapezoidal air intake using eddy resolving DES-method.

Novogorodtsev E.V. (TsAGI)

Abstract

As a result of flow compression in shock waves, wall friction, eddy formations and other phenomena, the flow in the inlet duct of the supersonic air intake becomes nonstationary and dynamic distortion appears. The dynamic distortion is quantified by the value of the root-mean-square parameter of the total pressure pulsations intensity ε that is calculated in the control section of the inlet duct. (ε is pulsating component of the total distortion parameter W= $\overline{\Delta\sigma_o}$+ ε, $\overline{\Delta\sigma_o}$ is the circumferential distortion parameter).
Numerical simulation of unsteady flow was performed using isolated trapezoidal intake configuration equipped with a boundary layer control system on the compression ramp surface. Numerical simulation of steady state flow was presented in [1-4]. To resolve the physical peculiarities of nonstationary turbulent flow, the modern eddy resolving DES (implemented in ANSYS CFX solver) method was applied. For three-dimensional viscous compressible flow computational modeling the geometry and the far field were discretized by means of spatial structured multi-block mesh. The mesh was generated manually, using the ICEM CFD software.
To evaluate DES method capability to predict parameter ε values, numerical results were compared with experimental data. CFD computation data were processed using standard experimental methodology adopted at TsAGI. It was established, that the parameter ε values, obtained with CFD computation in the inlet duct control section, coincide with the experimental data with a sufficiently high accuracy for all investigated operating conditions.

Keywords : *convergent air intake, total distortion parameter, root-mean-square parameter of the total pressure pulsations intensity.*

Nomenclature

W – Total distortion parameter
$\Delta\overline{\sigma_o}$ – Circumferential distortion parameter
ε – pulsating component of the total distortion parameter /root-mean-square parameter of the total pressure pulsations intensity
$q(\lambda_{cs})$ – Specific reduced mass flow in the control section
G_{cs} – Mass flow in the control section
T_{0cs} – Total temperature in the control section
F_{cs} – Control section area
P_{0cs} – Area averaged value of total pressure in the control section

1. Air intake geometry for numerical investigation

An image of mathematical model of supersonic trapezoidal air intake entrance and duct surfaces without boundary layer control system is depicted on Fig. 1.

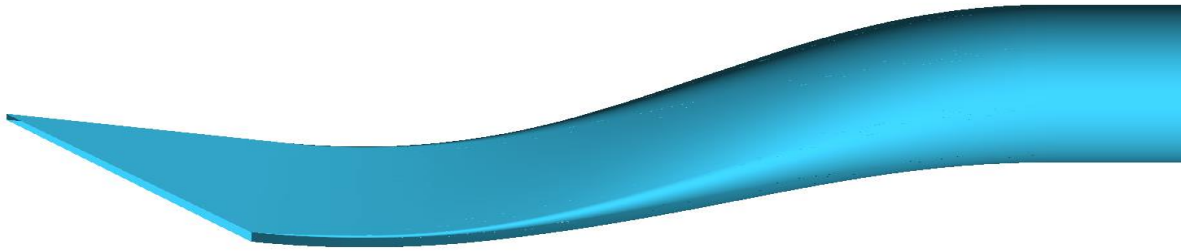

Fig.1 An image of supersonic trapezoidal air intake without boundary layer control system mathematical model

The mathematical model is a 1:10 scale with respect to the air intake of a full-size aircraft, an isolated air intake of a twin-engine maneuverable aircraft. To carry out a correct comparison of numerical results with experimental data, the scale of the mathematical model was chosen in accordance with the scale of the experimental trapezoidal air intake model made on its basis.

The inlet ramp configuration was designed using the gas-dynamic construction method. The preliminary supersonic flow compression carried out by a horizontal wedge with a straight edge, which is parallel to the edge of the shell and two side swept wedges. Because of the aircraft symmetry and in order to save time, only a left air intake was selected for the numerical simulation. The air intake is equipped with a curved S-shaped channel, bent in two planes. The cross section of the entrance to the engine was located in the plane perpendicular to the aircraft axis of symmetry. The numerical investigation was carried out both for the configuration of the air intake without the boundary layer control system, and for the configuration of the air intake with the boundary layer control system designed on the surfaces of the ramp. The configuration of the air intake with the boundary layer control system is depicted on Fig. 2.

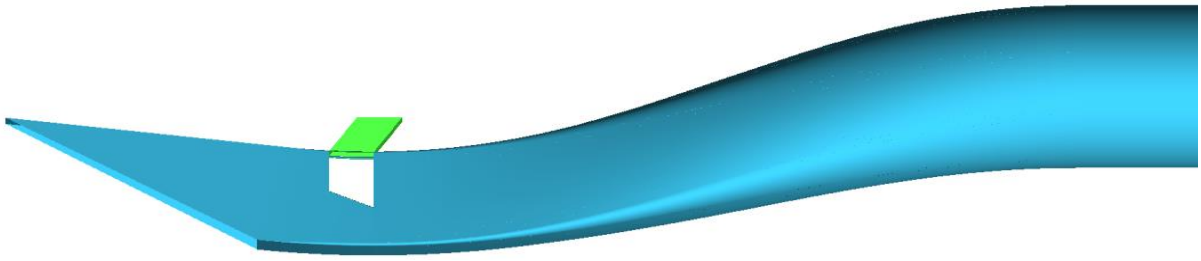

Fig.2 An image of supersonic trapezoidal air intake without boundary layer control system mathematical model

2. Numerical simulation method

2.1. Mesh and boundary conditions

For three-dimensional flow computational modeling a spatial multi-block structured hexagonal computational grid was constructed. The grid generation procedure was carried out manually using the ANSYS ICEM CFD software.

The computational domain includes the outer and inner parts of the air intake. The computational domain was bounded by a hemisphere-shaped surface in front, and by the plane behind. On the entire spherical surface, the inlet condition was established. Inlet conditions corresponded to the freestream flowing out from the nozzle of the TsAGI wind tunnel SVS-2. On the back side of computational domain the outlet boundary conditions was established. Outlet boundary condition corresponded to free flowing through the opening. At the boundaries corresponding to the solid surfaces, the non-flowing and no slip boundary conditions were established.

The computational grid consisted of about 10 million cells and was adapted for better resolving the boundary layer structure. The size of the first near-wall cell along the normal to the surface corresponded to the y+ parameter value of about 0.7. The block topology of a structured computational grid near the air inlet area is depicted on Fig. 3. This topology provided an opportunity to refine the grid near the solid surfaces of the walls. Also, this topology allowed to ensure the uniformity of the calculated grid, i.e. the corresponding dimensions of any two neighboring cells differ in no more than 1.2 times in size.

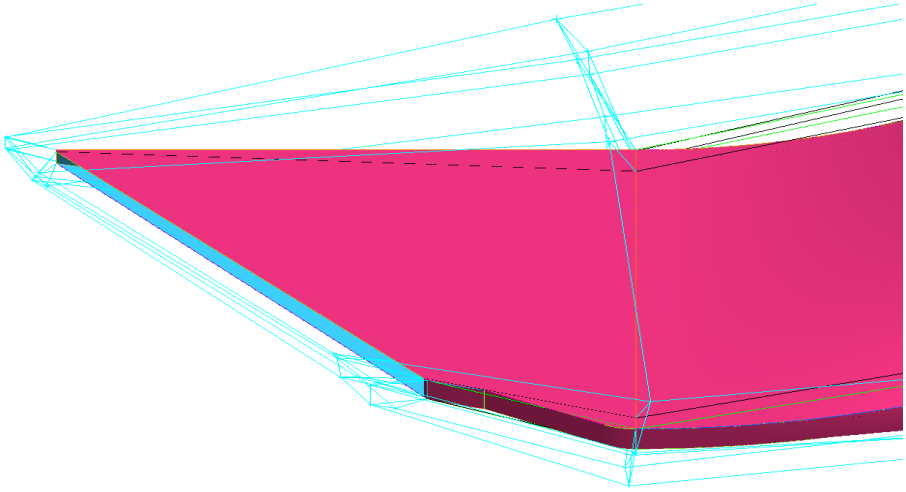

Fig.3 Computational grid near the inlet area block topology

2.2. Numerical data processing method

Using the unsteady flow in the air intake numerical simulation results, the flow parameters in the inlet duct control section are calculated. The root-mean-square parameter of the total pressure pulsations intensity ε characterizes the degree of non-stationarity of the total pressure field in the control section of the air intake channel. To calculate this the total pressure was calculated, in the process of unsteady numerical calculation, at each time step. Total pressure values were obtained at the points corresponding to the receivers of total pressure pulsations sensors. The scheme of the pulsation sensor receivers location in the control section of the experimental model is depicted on Fig. 4,. For the final parameter ε value calculation, the dependences of the total pressures on time at the four points were processed in accordance with the standard experimental method developed at TsAGI. It is worth noting, that the time step value selected for numerical calculation was $\tau = 10^{-5}$ s, which made it possible to ensure the stability of the numerical solution. Also this time step value provided acceptable time required to obtain the numerical data array necessary for estimating the ε parameter value. This time step value is also much lower than the pulsation sensors polling time in the experimental studies (the pulsation sensors polling frequency in the experimental study is about 6,750 Hz, which corresponds to the polling time $t_{exp} \sim 1.48 * 10^{-4}$ s)

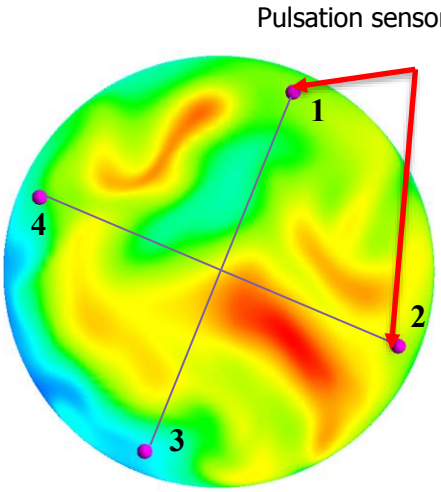

Fig.4 The scheme of total pressure pulsation sensor receivers in the inlet duct control section.

The air intake throttling was simulated using the duct constriction behind the control section plane (engine section) with an area F_{en}. The constriction was implemented as follows. Behind the air intake duct control section the Laval nozzle-shaped duct was formed. Directly behind the engine cross section, this duct had a cylindrical-shaped part with a cross-sectional area F_{en}. Than it was followed by constriction with a gradual transition to cylindrical section (washer) with the area F_w ($F_w < F_{en}$). The constriction wall profile was designed using the Vitoshinsky formula (see Fig. 5). The washer was followed by the duct expansion with transition to cylindrical part with the cross-sectional area F_{en}. The duct expansion was a mirror image of the constriction. Due to each point of the ε-parameter characteristic calculation the washer cross-sectional area varied. The duct constriction degree was characterized by the parameter $\overline{F_w}$, which is equal to the ratio of the washer cross-sectional area to the area of the engine section. The value of $\overline{F_w}$ was varied to obtain the parameter ε, in the cross section of the engine, as a function of the specific reduced air flow rate q (λ_{en}). The value of the specific reduced flow in the cross section of the engine $q(\lambda_{en})$ was calculated by the following formula:

$$q(\lambda_{en}) = \frac{G_{\text{en}} * \sqrt{T_{0\text{en}}}}{0.0404 * F_{en} * P_{0\text{en}}} \quad (1)$$

Here G_{en} is the air mass flow through the engine section, T_{0en} is the area-averaged total temperature in the engine section, F_{en} is the cross-sectional area of the engine section, P_{0en} is the area-averaged total pressure value in the engine section.

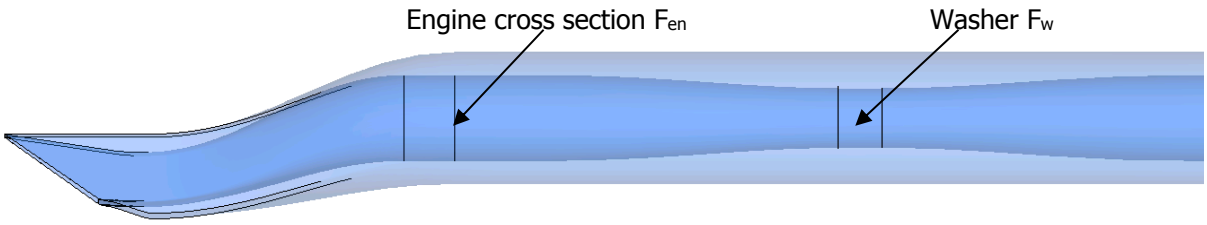

Fig.5 Duct throttling simulation scheme

2.3 Numerical simulation regimes

The isolated trapezoidal air intake flow in the wind tunnel model was numerically simulated. Investigated free-stream Mach number values were M=0, 0.7, 0.9, 1.8, the angle of attack and the

angle of sideslip were established to be zero. The M numbers regimes and air intake configurations are given in Table 1.

Table 1. Table of Mach number regimes and air intake configurations.

Regime number	Mach number	Air intake configuration
1	0	Without boundary layer control system
2	0.7	Without boundary layer control system
3	0.9	Without boundary layer control system
4	1.8	Without boundary layer control system
5	1.8	With boundary layer control system

3. Numerical simulation results

The total distortion parameter pulsation component plots as the functions of the specific reduced air flow rate through the engine sction for the five investigated Mach numbers depicted in the left part of Fig. 6.1 - 6.5. These plots were obtained both for numerical and experimnetal investigations. The instantaneous flow fields parameters such as pressure recovery for the M = 0 regime and the Mach number local values for the rest of the investigated regimes are depicted on the right part of these figures. Instantaneous flow fields were obtained in the numerical investigation. These fields clearly illustrate the main flow features of the regimes corresponding to the calculated $q(\lambda_{en})$.The fields are shown both in the longitudinal section of the air intake duct and in the duct control section. The comparison of dependences of the total pressure on time obtained in computational and experimental researches is depicted on the bottom of Fig. 7. Computational data were obtained at points 1,2,3,4 (see Fig. 4). The experimental data were obtained based pulsation sensors readouts. Pulsation sensors were installed on the experimental model according to the scheme shown in "Fig. 4". These dependences allow one to compare the pulsation intensity and frequencies obtained in the computational and experimental. This comparison was carried out for the operating modes of the air intake corresponding to the points C (calculated) and D (in the experiment). These points of the dependences of the parameter ε on q (λ_{en}) (see Fig. 7) correspond to the similar values of q (λ_{en}). These points correspond to the air intake operation in subcritical regimes and are located on the border of the air intake operation stability.

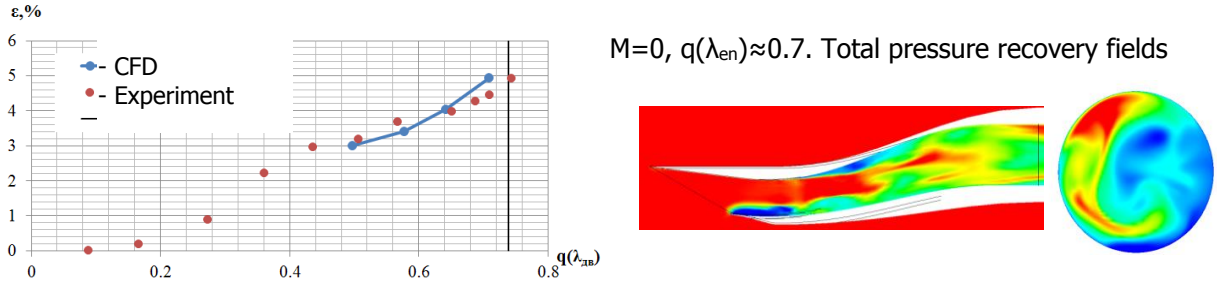

Fig. 6.1 Dependences of the parameter ε as a function of $q(\lambda_{en})$ and flow fields. Air intake configuration without the boundary layer control system. $M_\infty=0$.

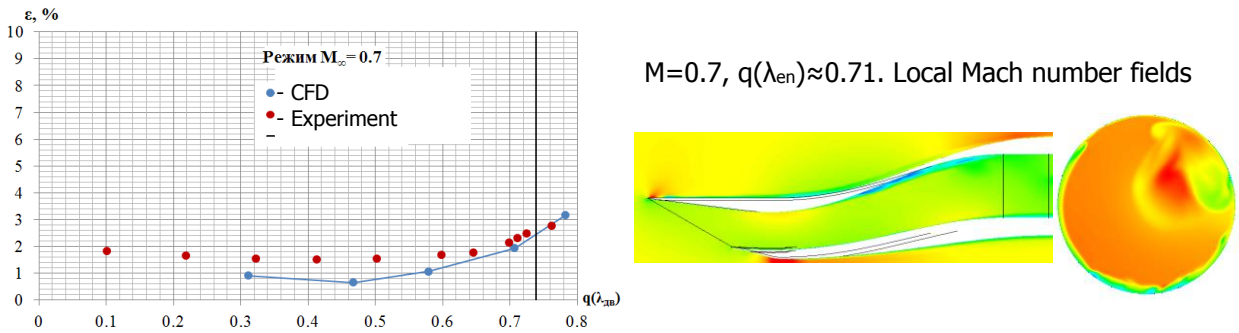

Fig. 6.2 Dependences of the parameter ε as a function of $q(\lambda_{en})$ and flow fields. Air intake configuration without the boundary layer control system. $M_\infty=0.7$.

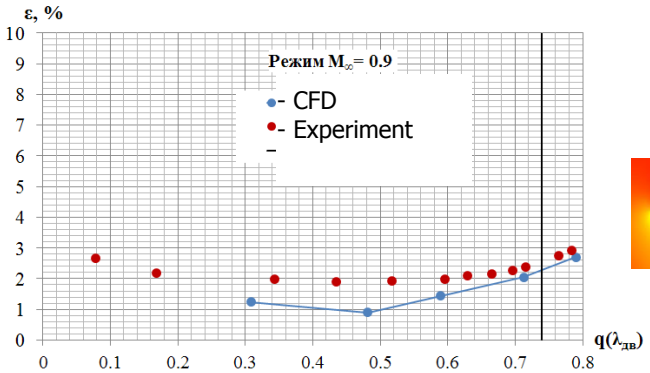

M=0.9, q(λen)≈0.71. Local Mach number fields

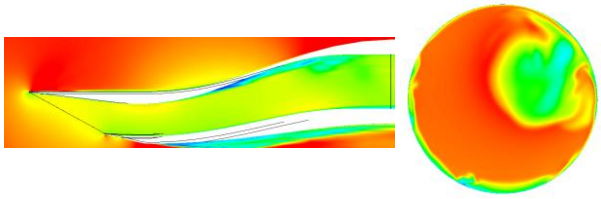

Fig. 6.3 Dependences of the parameter ε as a function of q(λen) and flow fields. Air intake configuration without the boundary layer control system. M∞=0.9, q(λдв)≈0.71.

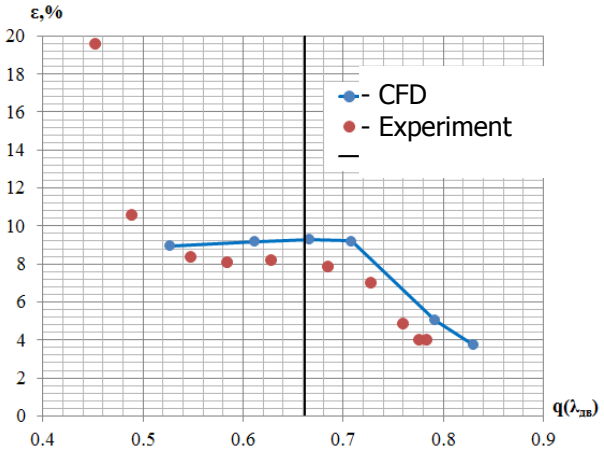

M=1.8, q(λen)≈0.66. Local Mach number fields

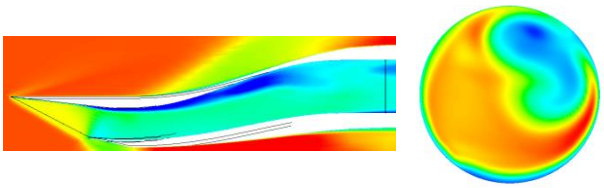

Fig. 6.4 Dependences of the parameter ε as a function of q(λen) and flow fields. Air intake configuration without the boundary layer control system. M∞=1.8

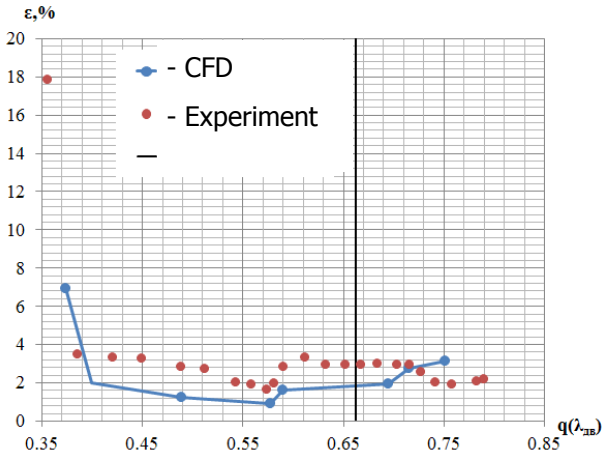

M=1.8, q(λen)≈0.59. Local Mach number fields

Fig. 6.5 Dependences of the parameter ε as a function of q(λen) and flow fields. Air intake configuration with the boundary layer control system. M∞=1.8

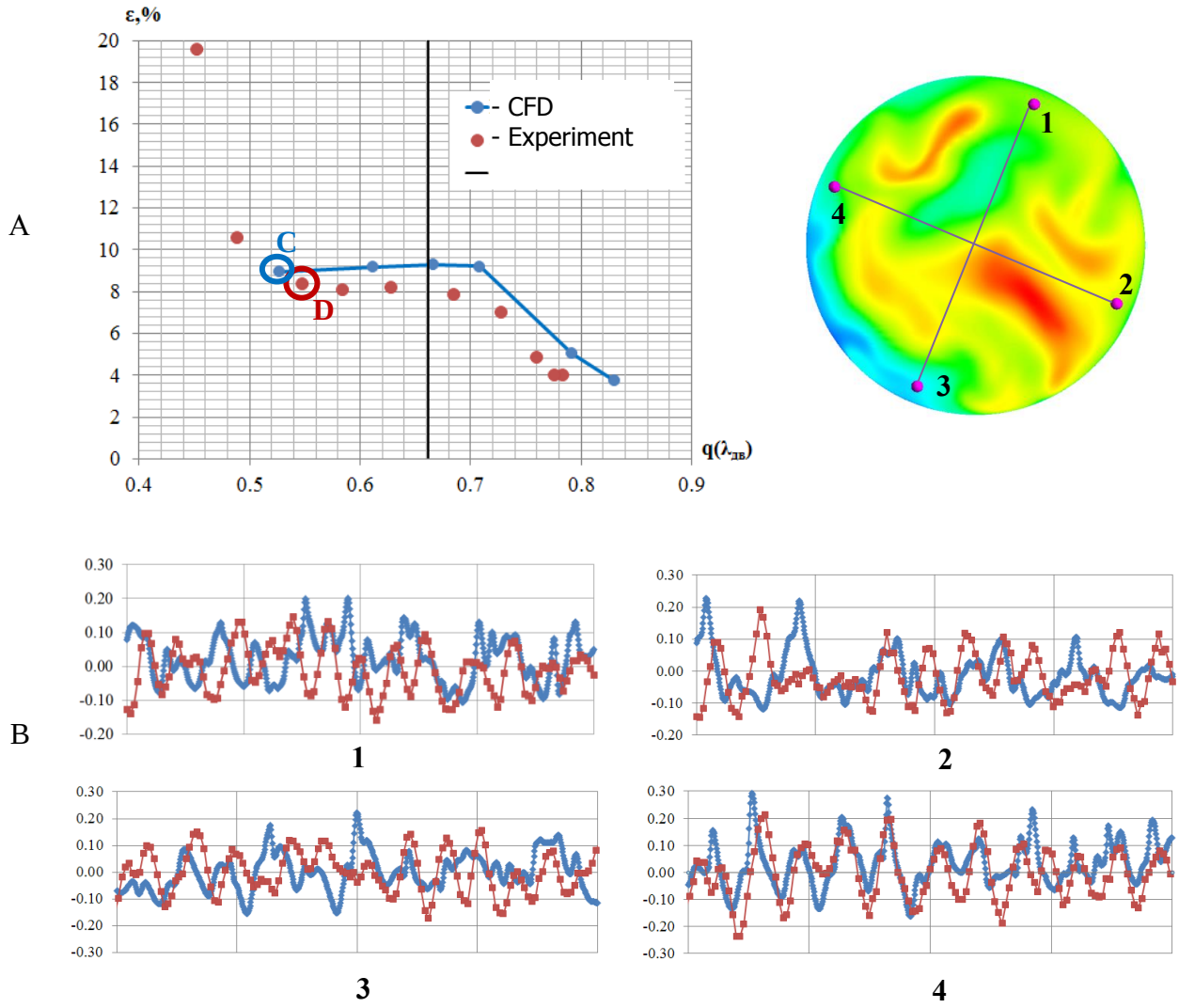

Fig. 7 Numerical and experimental total pressure pulsations comparisons. M_∞=1.8, air intake configuration without boundary layer control system

A) Averaged ε-parameter values.
B) Total pressure oscillation plots

3.1 Numerical results analisys

Let us consider the root-mean-square parameter of the pulsations intensity ε plots as a function of the specific reduced flow rate at the engine cross section q(λ_{en}). These plots are given in the left side of Fig. 6.1 - 6.5. Let us pay attention to the operating conditions corresponding to the Mach number $M_\infty = 0$ and $M_\infty = 1.8$, for the air intake configuration without boundary layer control system. The flow in the air intake duct under these operating conditions is characterized by the presence of large zones that occupy more than half of the engine diameter in cross section and are characterized by low total pressure recovery coefficient v values. These zones are vortex structures. The first vortex flow reasons in the $M_\infty = 0$ regime is the flow separation near the sharp edge of the inlet shell, due to the intense all-round suction of air into the air intake. The second reason is the flow separation in the diffuser part of the air intake duct with high curvature of the upper wall surface. The reason for the vortex structure presence for the operating condition $M_\infty = 1.8$ for the air intake configuration without the boundary layer control system is the flow separation due to shock-wave and boundary layer interference.

It is well known that the large eddies transfer process, caused by the flow separation in the air intake duct, is characterized by a high degree of nonstationarity and nonuniformity. Indeed, during the above-mentioned vortex structures passing through the pulsation sensor receiver (in experimental research) or through the corresponding point in the control section (in numerical simulation), the process oscillogram is recorded in the numerical and experimental researches (see Fig. 7). The parameter ε is a quantitative characteristic of the total pressure pulsations intensity. From the parameter ε plots (see "Fig. 6.1 - 6.4") in regimes corresponding to $M_\infty = 0$ and $M_\infty = 1.8$ for the air intake configuration without the boundary layer control system, the high levels for both experimental and computational ε parameter values were obtained (the parameter ε when $M_\infty = 1.8$ in the matching mode with the engine in the calculation obtained at the level $\varepsilon_c \sim 9\%$, in the experiment $\varepsilon_e \sim 8\%$). Thus, the magnitude of divergence between the dependences of the parameter ε on q (λ_{en}), obtained by calculation and experiment in these regimes does not exceed $\Delta\varepsilon_{max} \sim 1\%$, which indicates a sufficient numerical simulation results credibility degree.

The total pressure oscillograms, depicted on Fig. 7, vividly illustrate the total pressure oscillating process for four points in the control section. The challenging problem for supersonic air intakes computational and experimental research is the stability boundaries determination. The boundary between the air intake buzz mode and the stable mode may correspond to an intermediate so-called small instability mode. The small instability mode is characterized by the total pressure oscillations of the increased intensities and lower frequencies ($v \sim 30$ Hz for full-scaled air intake and 300 Hz for model-scaled air intake) compared with the air intake stable operation mode. Comparison of the numerical ocsillograms and experimental oscillograms was carried out for the small instability air intake mode corresponding to the selected points C and D in the plots depicted on Fig. 7. From the oscillogram comparison, it can be seen that the pulsations obtained by numerical and experimental researches for each of the four points are qualitatively similar both in intensity and in the frequencies.

To eliminate flow separation regions in the air intake duct for supersonic Mach number regimes the boundary layer control system is used. The boundary layer control system is designed in the form of transverse slits in the air intake throat area. The use of boundary layer control system for supersonic Mach number operating conditions (i.e. M = 1.8) significantly improves flow field in the air intake duct control section. Indeed, the parameter ε values for the air intake configuration with the boundary layer control system in the numerical research were $\varepsilon_c \sim 2\%$, and $\varepsilon_e \sim 3\%$ in the experimental research. These values were obtained for operating mode that corresponds to air intake and engine combined operation. The maximum value of divergence of computational and experimental dependences of the parameter ε on q (λdv) also does not exceed $\Delta\varepsilon_{max} \sim 1\%$. It should be noted that the maximum value of the divergence of the numerical and experimental data is realized in the area located to the left of the matching line, i.e. for smaller specific reduced flow in the engine cross section.

When the air intake operates at the modes corresponding to subsonic Mach numbers M = 0.7 and M = 0.9, the flow separated regions in the air intake duct are small in size. In this regard, the mean-square parameter of the pulsation intensity ε values in these modes were obtained $\varepsilon_c \sim 2.2\%$ (in computational research) and $\varepsilon_e \sim 2.5\%$ (in experimental research) for M = 0.9 and $\varepsilon_c \sim 2.5\%$ (in computational research) and $\varepsilon_e \sim 2.6\%$ (in experimental research) for M=0.7. These values also were obtained for operating mode that corresponds to air intake and engine combined operation.

The maximum divergence of the computational and experimental dependences of the parameter ε of $q(\lambda_{en})$ does not exceed $\Delta\varepsilon_{max} \sim 1\%$. At the same time, this discrepancy occurs in the area located to the left of the matching mode line, i.e. for operating conditions corresponding to the smaller specific reduced flow values. This discrepancy is apparently due to the fact that with an increase in the air intake throttling degree in subsonic flight modes there is a decrease in the flow rate in the air intake duct control section. For these modes, small-scale low-energy turbulent vortex formations contribute to the value of the mean-square parameter of the pulsations intensity ε. The resolution of such small vortex structures using computational grid with the above listed parameters seems to be difficult. In this regard, to further improve the accuracy of computational research and for more accurate understanding of the physical processes in an unsteady flow in the air intake duct, it is advisable to continue the numerical researches of this model using denser computational grid.

References

1.Efimov R.A., Karpov E.V., Novogorodtsev E.V. Trapezoidal air intake numerical simulation using RANS-method. In Proc .: Materials of the XXV Scientific-Technical Conference on Aerodynamics. Abstracts of February 27-28, 2014, TsAGI them. prof. N.E. Zhukovsky, pp.125-126.

2. Karpov E.V., Novogorodtsev E.V. Numerical simulation of flow in a trapezoidal air intake with a boundary layer control system. In the collection: Materials of the XXVI scientific and technical conference on aerodynamics. Abstracts February 26-27, 2015, TsAGI them. prof. N.E. Zhukovsky, pp. 131-132.

3. Karpov E.V., Novogorodtsev E.V. Computational and experimental researches of separated flows in the curved air intake duct of a maneuverable aircraft when operating on takeoff and landing flight modes. In Proc .: Proceedings of the XXVII Scientific and Technical Conference on Aerodynamics. Abstracts April 20-21, 2016.

4. Karpov E.V., Novogorodtsev E.V. Computational research of a flow divider installed in the curved air intake duct. In Proc .: Materials XXVIII scientific and technical conference on aerodynamics. Abstracts April 20-21, 2017, TsAGI them. prof. N.E. Zhukovsky, pp. 139-140.